Self-adaptive piezoelectric vibration absorber with semi-passive tunable resonant shunts

Jessé Paixão, Emmanuel Foltête, Emeline Sadoulet-Reboul, Gaël Chevallier, Scott Cogan

Self-adaptive piezoelectric vibration absorber with semi-passive tunable resonant shunts

Jessé Paixão[a,*], Emmanuel Foltête[a], Emeline Sadoulet-Reboul[a], Gaël Chevallier[a], Scott Cogan[a]

[a] *University of Franche-Comte, FEMTO-ST Institute, CNRS/UFC/ENSMM, Department of Applied Mechanics, 24 chemin de l'Epitaphe, Besancon, 25000, Franche-Comte, France*

Abstract

This paper proposes a novel self-adaptive strategy to control piezoelectric vibration absorbers (PVA) using a semi-passive resonant shunt with tunable inductance for vibration attenuation of harmonically excited structures. The tunable inductor is realized using ferrite cores and its inductance is controlled by means of the air gap effect between the cores using piezoelectric stack actuators. This device allows the control of the resonance frequency of the shunt circuit. The adaptive resonant shunt leverages the effect of antiresonance resulting from the electromechanical coupling of the structure with a resonant shunt with low electrical damping to attenuate the vibration of the harmonically excited structure. A machine learning control method based on a Gaussian process regression model is used to drive the tunable inductance based on minimizing the time-averaged RMS response of the structure. The experimental application of the proposed strategy is illustrated in an application to attenuate a single-mode of a simplified aircraft fuselage structure. A reduction of about 30% in the maximum vibration amplitude is observed by comparing the self-adaptive resonant circuit and a traditional resonant circuit designed based on the equal-peaks method.

Keywords: Adaptive shunt, Semi-passive resonant shunt, Piezoelectric vibration absorber, Tunable inductor, Machine learning control

1. Introduction

The growing demand for more efficient and environmentally friendly structures has led to a current trend toward lightweight structures, often more flexible and making them more susceptible to vibrations. This brings new challenges for current vibration control technologies, which must operate with increasing efficiency and contribute a minimum of mass to the structures on which they are installed [1]. In this context, one such technology that is gaining increasing interest are piezoelectric vibration absorbers (PVA). These devices, invented by Forward [2], employ piezoelectric transducers mounted on or even embedded in a primary

*Corresponding author

Email address: jesseag.paixao@gmail.com (Jessé Paixão)

structure to convert mechanical energy into electrical energy, which can be dissipated in an appropriate electrical circuit, called a shunt. The first shunt introduced by Forward [2] and one of the most famous is the so-called resonant shunt composed of a resistor and an inductor connected in series or parallel. Since then, different types of passive and active shunt circuits have been developed for single and multi-mode damping of vibrations [1].

The theoretical foundations for the design of resonant PVA shunts were laid by Hagood and Flotow [3] based on the equal-peak design method developed for dynamic vibration dampers (DVA), which is considered to be an equivalent mechanical system. This method provides an approximate solution of values for resistance and inductance to the optimization problem defined by minimizing the H_∞-norm of the system's frequency response function (FRF) considering a single mode. Recently, an analytic closed-form solution to this optimization problem was proposed by Soltani et al. [4]. Several other methods for designing resonant circuits have been investigated and proposed in the literature, including more complex shunts and multiple modes of vibration [5, 6]. Most of these methods focus on broadband frequency excitation, with the objective of attenuating single or multiple vibration modes as much as possible. Fundamentally, they rely on tuning the electrical resonance frequency to the desired mechanical resonance frequency, in order to maximize the transfer of vibration energy from the primary structure to the shunt circuit, where it is dissipated through electrical damping. Although PVA with resonant shunts can provide an important vibration attenuation for low frequency modes, small variations in the resonance frequency of the shunt or the primary structure cause substantial performance degradation [7, 8].

In view of this problem many studies have investigated PVAs with adaptive resonant shunts, which are circuits capable of performing on-line adaptation of their impedance [1]. This type of device is commonly used to improve the robustness of piezoelectric absorbers in operation, which are very sensitive to uncertainties due to operational and environmental conditions. The adaptive shunt circuit is able to change its properties to compensate for possible effects of variation in its resonance frequency or of the structure, improving the robustness of the vibration attenuation performance. For the design of an adaptive shunt two elements are essential: a mechanism to drive its natural frequency and a strategy of control. Hollkamp and Starchville [9] were the pioneers to propose a PVA with an adaptive shunt, capable of automatically adjusting to the resonance frequency of a defined vibration mode using a motorized potentiometer and a synthetic inductor. They proposed a control strategy based on the minimization of the root mean squared value of the time-vibration signal by gradient-search algorithm. Fleming et al. [10] applied a control strategy for the single-mode shunt damping in a cantilevered beam structure using a synthetic impedance controlled by adjusting the relative phase difference between the velocity and the electrical current flowing in the shunt, which was later extended to multi-mode shunt damping by Niederberger et al. [11]. Gripp et al. [12] explored the use of a negative capacitance with an adaptive resonant shunt, controlled by the relative phase difference between velocity and electrical current, to improve the attenuation robustness of the PVA in the face of variations in the natural frequency of the host structure. They demonstrated a significant gain in attenuation performance of this circuit in a shell structure compared to a purely adaptive resonant shunt. More recently, Gardonio et al. [13] demonstrated that minimizing the time-

averaged vibration response of a mechanical system with a PVA when the system is excited by a stochastic force is equivalent to maximizing the time-averaged electric power dissipated by the resonant shunt, which is characterized by a bell-type non-convex surface with a single maximum. From this result they developed an adaptive shunt using a controller based on the extremum seeking algorithm capable of adjusting online the resistance and inductance emulated by an synthetic impedance to maximize the time-averaged electric power dissipated by the PVA [14]. In addition to adaptive shunts, which are usually based on active circuits, switching shunts based on semi-active circuits such as state switching and synchronized switch damping have also been explored in the literature to improve the PVA robustness [15–18]. The major drawbacks of switching shunts are the high order frequency signals required to control the switching circuits and the acoustic disturbances during operation [1].

The adaptive PVA shunts proposed in the literature are mostly oriented to structures excited in a broad frequency band, aiming to ensure near-optimal attenuation independent of variations in the natural frequencies of the structure's modes, which usually leads to a frequency response function with two equal-peaks. On the other hand, in harmonically excited structures, minimizing the vibration amplitude at each frequency leads to an even more efficient solution by tuning the electrical resonance frequency to the excitation frequency and decreasing the electrical damping as much as possible, creating an anti-resonance [19]. For very low damping, this anti-resonance can practically cancel the steady state vibration amplitude of the structure. This effect can be exploited with adaptive shunt circuits capable of tuning their electrical resonance frequencies by changing their parameters to attenuate structures excited with time-varying harmonic signals. This strategy, known as antiresonance locus, was recently exploited by Audeley et al. [19, 20] in an electromagnetic vibration absorber with adaptive resonant shunt controlled by an electronic chopper with pulse-width modulation. Despite being a well established strategy in the literature and already explored for electromagnetic vibration absorbers, the experimental application of the antiresonance locus strategy to absorbers based on piezoelectric transducers has not yet been investigated and proves to be challenging because the required reduction in the electrical damping reduces the robustness and stability margin of the structure, hindering the design of a suitable controller, and it also increases the energy flowing through the shunt circuit. This latter issue hampers the application of active circuits commonly used in adaptive shunts, such as virtual inductors realized for example using Antoniou's circuit [21] or Riordan's gyrators [22], or synthetic impedance circuits [23]. Although these active circuits provide a remarkable electrical frequency adaptability, they suffer from saturation limits often related to their operational amplifiers. Details of the saturation issues faced by virtual inductors and synthetic impedances, as well as the delay-induced instabilities of the latter, are discussed in Dekemele et al. [24] and Raze [25] respectively. In this context, a novel semi-passive resonant shunt is proposed in this work to enable the application of the antiresonance locus strategy using piezoelectric transducers for vibration attenuation, which has the potential to substantially reduce the mass added to the primary structure compared to electromagnetic transducers, since they are lighter and the resonant circuit that presents more weight can be positioned outside the structure through the electrical connection.

The control of PVA with adaptive shunts mostly relies on traditional control approaches

based on system identification to design a controller, and then depend on accurate model descriptions to enable safe and high performance control. This process can be time-consuming and a complex endeavor in the presence of nonlinearities. Machine learning methods can circumvent this process by learning the system's input-output characteristics directly from data, offering a significant potential for control, which although have been extensively explored in the past years in robotic applications [26, 27], to the author's best knowledge has not been yet explored in PVA. A machine learning control approach using a Gaussian Process Regression model (GPR) is investigated in this work in the development of a self-adaptive PVA based on the anti-resonance locus strategy for vibration attenuation of harmonically excited structures. It is important to note that the self-adaptive capability is fundamentally different from that applied in PVA with traditional adaptive shunts, as the system learns how to adapt to changes in excitation frequency by itself through the machine learning model. This type of self-adaptive or self-learning strategy has recently been explored in the literature for other vibration control techniques. Wang et al. [28] proposed a self-learning tuning method based on neural networks for an electromagnetic vibration absorber with negative stiffness under variable frequency excitation. Song et al. [29] investigated the use of a nonlinear autoregressive with exogenous input model for vibration identification and control of a flexural beam with piezoelectric actuators. A similar approach using a GPR model was recently explored by Maiworm et al. [30, 31] in a control framework for scanning quantum dot microscopy.

In this paper, we propose a self-adaptive PVA with semi-passive resonant shunt for vibration attenuation of structures subjected to time-varying harmonic excitations. The main objective of this paper is to circumvent the above-mentioned challenges in developing this type of device and to demonstrate the experimental application for vibration attenuation in a demonstrator. We present the development of a tunable resonant shunt composed of a passive inductor with movable ferrite cores and low internal resistance. A simple mechanism to control its inductance and consequently the electrical resonance frequency of the shunt is proposed based on the use of voltage-driven piezoelectric stack actuators to control the air gap between its ferrite cores. A machine learning approach to control this device based on GPR model is investigated. This model is used in an offline step for supervised learning of the control signal applied to the resonant shunt to minimize the vibration of the main structure as a function of the excitation frequency, thus providing the self-adaptive capability of its electrical resonance frequency to the time-varying tonal excitation for real-time control. Therefore, the self-adaptive PVA proposed in this work, which seeks to attenuate vibration based on the anti-resonance locus strategy using the ML control algorithm, requires, in addition to the piezoelectric patch connected to the tunable semi-passive shunt circuit, a second piezoelectric sensor patch on the structure used as a sensor and a digital processing unit to execute the control algorithm. The potential range of applications of the self-adaptive PVA investigated here, which is limited to harmonically excited structures, targets propulsion systems, such as propellers or turbofan engines, and rotating machinery in general.

This paper is organized as follows: in Section 2 a lumped mass model of a single-degree-of-freedom structure connected to a resonant shunt is reviewed and is used to present the theoretical foundations of the strategy for vibration attenuation of harmonically excited

structures based on antiresonance locus. A brief description of the semi-passive tunable resonant shunt development and the theoretical concept behind the inductance tuning device based on the air gap between the movable ferrite cores is presented. Then, the self-adaptive control strategy based on the GPR model for the implementation of closed-loop system is presented. The experimental setup for applying the proposed methodology on the demonstrator and the results obtained are presented and discussed in Section 3. Finally, the conclusions are summarized in Section 4.

2. Piezoelectric vibration absorbers

In this section a lumped mass model of a structure connected to a PVA with resonant shunt is presented. This simplified model is sufficient to show the fundamentals of the operation and design of a PVA, as well as the adaptive strategy for vibration attenuation of harmonically excited structures. The fundamentals for the design of the tunable inductance are presented and discussed. Finally, the complete self-adaptive strategy for online control of the system is proposed.

2.1. Lumped parameter model of structure with piezoelectric vibration absorber

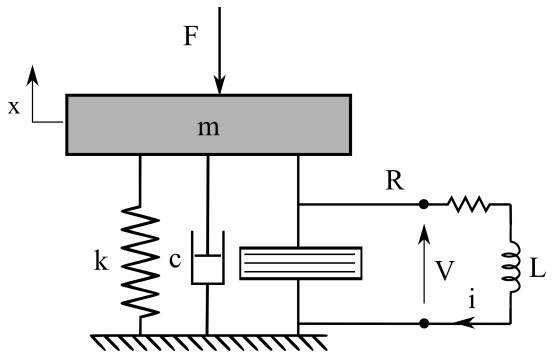

Figure 1: Lumped mass model of the structure with the piezoelectric vibration absorber.

The lumped mass model of a structure coupled to a piezoelectric transducer connected to a resonant shunt composed of an inductor and a resistor in series is schematically represented in Figure 1. An external force F is applied to the structure, causing a mechanical displacement x and a voltage V across the electrodes of the transducer. The governing equations of the coupled mechanical and electrical systems are given by [25]:

$$\begin{cases} m\ddot{x} + c\dot{x} + k_{oc}x - \theta q = F \\ L\ddot{q} + R\dot{q} + \dfrac{1}{C^{\varepsilon}}q - \theta x = 0, \end{cases} \tag{1}$$

where m, c, k_{oc} represent the mass, damping and stiffness of the structure when the transducer is open-circuited (including the mechanical stiffness of the piezoelectric component), q is the electric charge displacement, θ is the piezoeletric coupling coefficient and C^{ε} is the piezoelectric capacitance at constant strain.

The electromechanical coupling factor of this system is defined based on the mechanical behavior considering open-circuit ($q = 0$) and short-circuit ($V = 0$) electrical boundary conditions, and it is given by:

$$k_{\mathrm{c}} = \sqrt{\frac{\omega_{\mathrm{oc}}^2 - \omega_{\mathrm{sc}}^2}{\omega_{\mathrm{sc}}^2}} \tag{2}$$

where ω_{oc} and ω_{sc} are the resonance frequencies of the structure with the transducer in open-circuit and short-circuit configurations respectively, and are defined by:

$$\omega_{\mathrm{oc}} = \sqrt{\frac{k_{oc}}{m}} \quad \text{and} \quad \omega_{\mathrm{sc}} = \sqrt{\frac{k_{sc}}{m}} = \sqrt{\frac{k_{oc} - \theta^2 C^{\varepsilon}}{m}} \tag{3}$$

where k_{sc} is the structural stiffness when the transducer is short-circuited.

The electromechanical coupling defined by Equation 2 is an important factor considered for shunt circuit design because it represents the efficiency of strain energy conversion into electrical energy. Furthermore, it can be easily identified experimentally through the frequencies of the structure in open and short-circuit, which allows to mitigate modeling uncertainties [25].

The dynamic behavior of the electric circuit RL can be characterized by the resonance frequency (ω_e) and the electrical damping (ξ_e), which are obtained by:

$$\omega_e = \frac{1}{\sqrt{LC^{\varepsilon}}}, \quad \xi_e = \frac{R}{2}\sqrt{\frac{C^{\varepsilon}}{L}} \tag{4}$$

The frequency response function of this model can be computed from the Fourier transform of the Equation 1 and results in:

$$H(\omega) = \frac{X(\omega)}{F(\omega)} = \frac{-\omega^2 L + \mathrm{i}\omega R + \frac{1}{C_p^{\varepsilon}}}{\left(-\omega^2 m + \mathrm{i}\omega c + K_{oc}\right)\left(-\omega^2 L + \mathrm{i}\omega R + \frac{1}{C^{\varepsilon}}\right) - \theta^2} \tag{5}$$

where $X(\omega)$ is the Fourier transform of x, $F(\omega)$ is the Fourier transform of F and $\mathrm{i} = \sqrt{-1}$.

Based on the FRF, the problem of vibration attenuation considering a broadband excitation can be described as an optimization problem, where one wants to minimize the H_∞-norm, for example the FRF maximum amplitude. The solution of this optimization problem considering the FRF displacement/force leads to an approximation for the optimal inductance and resistance values [6]:

$$L_{ep} = \frac{1}{C^{\varepsilon}\omega_{\mathrm{oc}}^2} \quad \text{and} \quad R_{ep} = \sqrt{\frac{3}{2}}\frac{k_{\mathrm{c}}}{C^{\varepsilon}\omega_{\mathrm{oc}}} \tag{6}$$

This solution shows no significant difference for systems with low structural damping (below 10%) as demonstrated by Thomas et al. [6]. It leads to a FRF with two peaks of equal amplitudes around the resonance frequency of the mechanical system with a substantial amplitude attenuation compared to the system with an open-circuit transducer (or without PVA) as presented in Figure 2. However, small variations in the properties of the shunt

or the structure can cause an important increase in the maximum amplitude. It should be remarked that this solution considers a broadband frequency excitation near the mode and constant properties of the shunt.

2.2. Adaptive shunt based on antiresonance locus

In considering a harmonic excitation of the structure of known frequency Ω and an adaptive resonant shunt in which the inductance and resistance can be varied, a more efficient attenuation can be obtained using a different strategy, the antiresonance locus [20]. This strategy can be inferred from the FRF presented in Equation 5. The electromechanical coupling of the transducer induces a term in the numerator of the equation. For a given excitation frequency (Ω) and assuming null electrical resistance, one can show from Equation 5 that the FRF is zero for :

$$L_{adaptive} = \frac{1}{C^{\varepsilon}\Omega^2} \tag{7}$$

This occurs due to the existence of an antiresonance, in which the excitation force counteracts the force generated by the electromechanical coupling, making the structure remain at rest [20]. It should be noted, however, that this case of complete vibration attenuation of the structure at rest is purely theoretical as it would imply an infinite current in the circuit. In practice, although significant vibration attenuation can be achieved, it is limited. By increasing the electrical resistance in the circuit, some of the energy is dissipated as heat, reducing the attenuation effect on the antiresonance. If the electrical resistance remains small, the maximum attenuation is obtained for the inductance given by Equation 7, for which $\Omega = \omega_e$. Therefore, by applying this strategy for a harmonic excitation varying within a frequency range one can drastically attenuate the vibration amplitude of the structure as presented in Figure 2.

The application of this strategy depends on controlling of the resonance frequency of the electrical circuit through the inductance and a circuit with low electrical resistance. Although these two issues can be solved using a synthetic impedance to emulate the resistance and the inductance, this type of active circuit has instability problems along with other limitations already discussed previously. To circumvent these limitations, we propose the use of a semi-passive device that will be discussed in the next subsection.

2.3. Semi-passive tunable inductor

A passive inductor is a simple device, typically consisting of a coil of wire, which can be wound around a core made of different materials such as iron, ferrite, or air. This electrical component stores energy in a magnetic field when a current flows though the coil. The great difficulty in using passive inductors in PVA is related to the high values of inductance required for attenuation of low frequency modes - usually in the order of tens of H - which are difficult to find commercially or present impractical dimensions [32]. Nevertheless, Lossouarn et al. [32] recently demonstrated the feasibility of more compact high-value passive inductors using ferrite cores with high magnetic permeability. Although this allows the fabrication of the inductors necessary for the resonant circuit, these devices have constant inductance. In

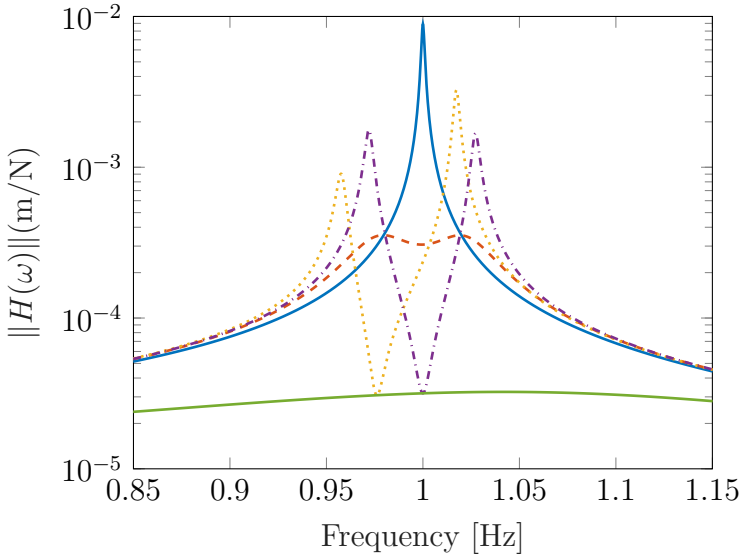

Figure 2: Frequency response function of primary system with an open-circuit transducer (—) and with resonant shunt circuit : $L = L_{ep}$ and $R = R_{ep}$ (- -); $L = L_{ep}$ and $R = 0.1R_{ep}$ (-·-); $L = 0.9L_{ep}$ and $R = 0.1R_{ep}$ (····); $L = \frac{1}{C^{\varepsilon}\Omega^2}$ and $R = 0.1R_{ep}$ (—). A mechanical damping ratio of 0.08 % is considered for the system with open-circuit shunt.

order to realize a device with tunable inductance, necessary to implement the antiresonance locus strategy, we will investigate the effect caused by the air gap between the ferrite cores.

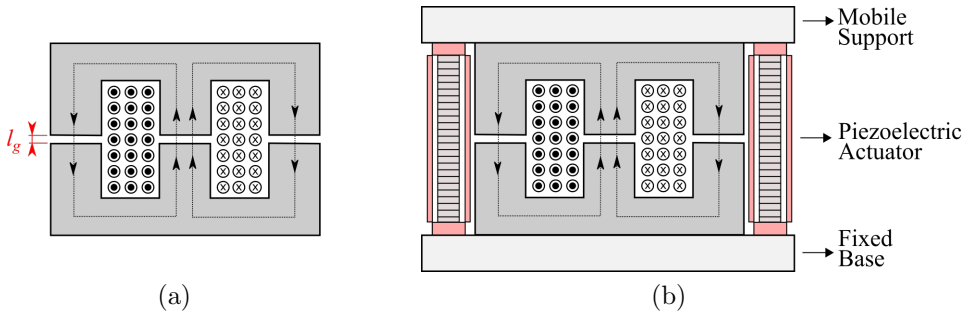

Figure 3: Inductance with air gap scheme.

The effects of the presence of an air gap between the cores of the inductors have been well studied in the literature. It is commonly exploited to improve the design of these devices, since it increases the saturation current, allows the storage of more energy, and decreases the sensitivity of the inductor to variations in the magnetic properties of the cores [33]. For the inductor illustrated in Figure 3(a), under assumption of a homogeneous flux density distribution, the inductance and air gap l_g are related by $L = C_1/(C_2 + C_3 l_g)N^2$, where N is the number of turns in the coil, and C_1, C_2 and C_3 constants are related to inductor's dimensions and physical properties as discussed Darleux [34]. Indeed, the inductance can be controlled by the air gap between the cores. It is important to note that this linear

relationship is valid under the assumption of a homogeneous flux density distribution, which is reasonable for a small air gap. However, as the gap increases, the magnetic flux lines begin to bulge, causing the effective reluctance of the air gap to decrease and the inductance to increase in a non-linear relationship, a phenomenon known as the fringe effect. For more details on the fringe effect, the interested reader may refer to [33, 35].

Small variations in the air gap can cause significant variations in inductance, thus requiring a precise control mechanism. For this purpose, we propose the use of the system illustrated in Figure 3(b) composed of two piezoelectric stack actuators capable of controlling the air gap between the cores with micrometer precision and two mechanical supports attached to the cores. The piezoelectric stack actuators allow the upper core to be displaced by the force transmitted through the mobile support. The displacement is imposed by applying a constant voltage on the piezoelectric stacked actuators.

2.4. Self-adaptive PVA based on machine learning control

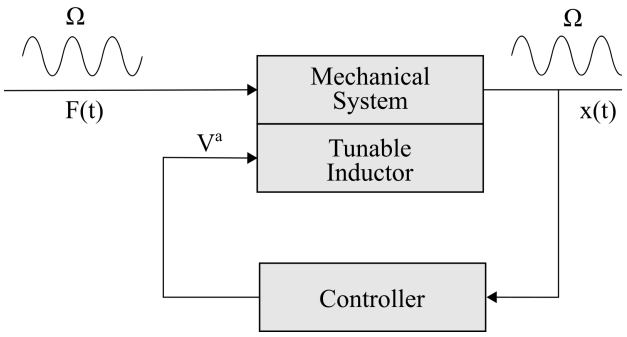

Figure 4: General schematic representation of the closed-loop control structure.

Having designed the semi-passive tunable inductor presented in the previous subsection, it can be used in a closed-loop system to implement the vibration attenuation based on the antiresonance locus approach. A diagram with all of the components of this system is illustrated in Figure 4. Recall that the main goal of the self-adaptive strategy proposed here is to minimize the vibration of the mechanical structure for a given harmonic excitation by controlling the tunable inductance through the applied voltage on the piezoelectric stack actuators.

As discussed for the simplified lumped mass model, the solution of this optimization problem is based on the strategy of an antiresonance locus considering a small resistance and adaptive inductance, leading to Equation 7, where the optimal inductance depends on the excitation frequency and represents the condition in which the frequency of the electrical circuit coincides with the excitation frequency. Although this solution can be directly related to the mechanism of inductance tuning through the air gap between the ferrite cores, it is important to note that this variable is driven by the voltage applied to the piezoelectric actuators, which has an unknown relationship with the air gap. To address this problem, we propose an approach based on machine learning control.

Machine learning control has recently been formalized by Duriez et al. [36] as a generic model-free strategy for controlling nonlinear systems, although one of the first works using this type of technique was reported by Fleming and Purshouse [37] in the past. In this approach, the control problem is formulated as an optimization with respect to a cost function that can be evaluated using the system's measured outputs. The control objective is to minimize the defined cost function within the space of the control laws. The controller is formulated based on a machine learning algorithm that is trained on an off-line learning loop using data from simulations or experiments. It is then used to minimize the objective in the online closed-loop control system [38]. Different machine learning algorithms have been used with this approach, including: genetic algorithms, reinforcement learning, artificial neural networks, and support vector machines [36, 39].

In this paper we propose to use the Gaussian process regression (GPR) model, a machine learning algorithm that has attracted attention due to its stochastic formulation and ability to describe nonlinear functions. We propose to use the GPR model in an off-line loop for the supervised learning, where a training data set under operational conditions is provided and the model learns by itself the relationship between the observed variables, which is a priori unknown. This model is then used in the closed-loop system using a controller, based on the machine learning approach to determine the applied voltage for each excitation frequency, in order to minimize the vibration amplitude of the structure. This novel self-adaptive strategy to control the resonant shunt is illustrated in Figure 5 and presented in detail in what follows.

In the problem presented in this paper, the cost function is the time-averaged RMS of the vibration of the mechanical system, which is assumed to depend only on the excitation frequency (Ω) and the applied voltage of the piezoelectric actuators (V^a) of the tunable inductance, and is expressed as $J(\Omega, V^a)$. This hypothesis is supported by the linear vibration behavior of the structure for the applied excitation level. Additionally, environmental uncertainties, such as temperature variation, which can also impact this cost function, are not considered. This type of cost function was already explored with adaptive resonant shunts and is justified by its smooth behavior, less susceptible to noise than the maximum vibration amplitude, and the existence of a global minimum point as reported by Fleming and Moheimani [10].

Consider a data set available for training with noisy observations of the time-averaged RMS response $\mathbf{J} = [J_1, \ldots, J_N]^T$ of the mechanical system for a set of applied actuator voltage $\mathbf{V^a} = [V_1^a, \ldots, V_N^a]^T$ and excitation frequencies $\mathbf{\Omega} = [\Omega_1, \ldots, \Omega_N]^T$. Adopting the notation of Rasmussen[40], let $\mathbf{x} = [\mathbf{V^a}, \mathbf{\Omega}]^T$ denote a matrix of multivariate training inputs, and $\mathbf{y} = [\mathbf{J}]$ denote the corresponding vector of training outputs. Assuming that these observations can be expressed following regression model :

$$y_i = f(x_i) + \varepsilon, \quad \varepsilon \sim \mathcal{N}\left(0, \sigma_n^2\right) \tag{8}$$

where f is a unknown function and ε is a Gaussian distributed noise with zero mean and variance σ_n^2. Various methods can be used to solve this classic regression problem. We propose in this work to apply the Gaussian Process regression (GPR) model, a non-parametric

stochastic model that has been recently explored for control problems of this type. Thus, the function f can be written as:

$$f(\mathbf{x}) \sim \mathcal{GP}\left(m(\mathbf{x}), k\left(\mathbf{x}, \mathbf{x}'\right)\right) \tag{9}$$

where $m(\mathbf{x})$ and $k\left(\mathbf{x}, \mathbf{x}'\right)$ are respectively the mean and covariance functions of the distribution over functions described by the Gaussian process.

The main aim of the GPR model is to make predictions for new input data that are not in the training data. Given a new input vector, $\mathbf{x}_*$, one can estimate the distribution over functions of a new point y_* given the previous observations as :

$$f_*(\mathbf{x}_*) \sim \mathcal{N}\left(m_*\left(\mathbf{x}_*\right), k_*\left(\mathbf{x}_*, \mathbf{x}_*\right)\right) \tag{10}$$

where

$$\begin{aligned} m_*\left(\mathbf{x}_*\right) &= k_*^T\left(\mathbf{x}^*, \mathbf{x}\right)\left[K\left(\mathbf{x}, \mathbf{x}\right) + \sigma_n^2\mathbf{I}\right]^{-1}\mathbf{y}, \\ k_*\left(\mathbf{x}_*, \mathbf{x}_*'\right) &= k\left(\mathbf{x}_*, \mathbf{x}_*\right) - k\left(\mathbf{x}_*, \mathbf{x}\right)^\top\left(K + \sigma_n^2\mathbf{I}\right)^{-1} k\left(\mathbf{x}, \mathbf{x}_*\right). \end{aligned} \tag{11}$$

are the posterior mean and variance of the GPR model, $\mathbf{I}$ is the identity matrix, σ_n^2 is the variance of the noise and K is a matrix whose i,j-th element is given by the covariance function $k(x_i, x_j)$. An effective and common choice for the covariance function is the squared-exponential function which is adopted in this paper. The hyperparameters of the GPR model comprising the noise signal (σ_n^2) and length-scale of the squared-exponential covariance function are obtained through the maximization of the marginal likelihood function using a gradient-based optimizer based on the Sequential Least Squares Programming method. This traditional procedure for training the GPR model is not detailed here for the sake of clarity. The interested reader is invited to consult [40, 41] for more details. In addition, the code used for implementation is available on the github repository[1].

Assuming that the posterior mean of GPR model adequately represents the cost function $J(\Omega, V^a)$, it can be used to control the voltage applied to the piezoelectric actuators in order to minimize the vibration of the structure by solving the following minimization problem:

$$\bar{V}^a(\Omega) = \underset{V^a}{\operatorname{argmin}}\; m_*(\mathbf{\Omega}, \mathbf{V^a}) \tag{12}$$

This problem can be solved for a given excitation frequency by interpolating the GPR model within the training domain and selecting the voltage to be applied to the piezoelectric actuators that provides the lowest value for the cost function. The complete closed-loop system based on the machine learning control approach is presented in the diagram of Figure 5. In the training step of the GPR model, which is carried out offline, the excitation frequency and the applied voltage are varied throughout the training domain and the cost function is obtained experimentally by calculating the RMS value of the system response for each operational condition. The excitation frequency is estimated from the system response

[1] https://github.com/jessepaixao/SPARTA

signal using the fast Fourier transform based on the parabolic interpolation approach, which provides improved frequency resolution for harmonic signals [42]. It is important to note that in the closed-loop operation of the control system, only the excitation frequency is used as the input variable of the trained GPR model, which is used to estimate the voltage value that minimizes the cost function. Additionally, it should be emphasized that the trained GPR model provides an approximation of the cost function within the training domain and is only valid for closed-loop operation under the training conditions.

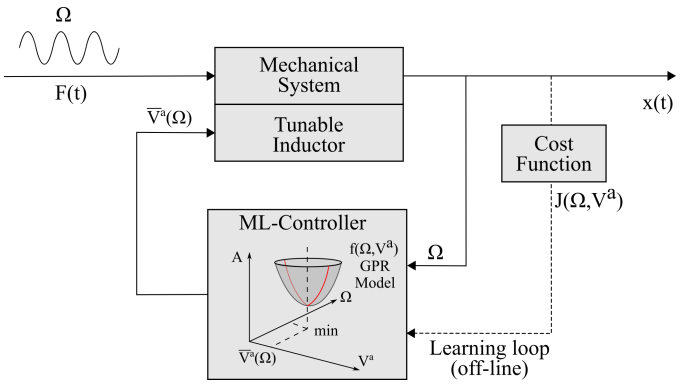

Figure 5: Proposed self-adaptive strategy for the the closed-loop operation of the PVA with semi-passive tunable inductor based on the machine learning control approach using GPR model for vibration attenuation of a harmonically excited structure.

3. Experimental validation of the self-adaptive vibration absorber

In this section the experimental application of the proposed strategy is presented for a simplified aircraft prototype. This mechanical structure is used only as a demonstrator for the validation of the methodology for vibration reduction. The design and realization of the resonant shunt and the passive tunable inductor are discussed. Then, the self-adaptive strategy is utilized for the vibration attenuation of the airplane prototype considering a swept harmonic excitation and the results obtained are discussed.

3.1. Experimental Setup

A photograph of the experimental apparatus is provided in Figure 6(a). The simplified aircraft mockup was suspended on a test rig by flexible cables to simulate free-free boundary conditions. Two piezoelectric patches were glued to the airplane wings, the first used for vibration attenuation connected to the shunt circuit, denoted PZT2, and another employed as a collocated sensor to measure the voltage, denoted as PZT1. A schematic representation detailing all components and the integration of the experimental setup is shown in Figure 6(b), where three subsystems can be identified: the so-called testing subsystem highlighted in red, responsible for the excitation and vibration measurement of the structure to perform the tests; the named control subsystem highlighted in blue, an active circuit responsible for controlling the shunt circuit; and lastly the resonant shunt subsystem highlighted in green, a passive circuit.

The testing subsystem is managed by a computer dedicated to signal analysis and integrated with the Polytec controller. The structure is excited using an electrodynamic shaker positioned close to PZT 1 and the applied excitation force is measured using a load cell PCB type 208C01. The transverse velocity is measured at the point shown in Figure 6(b), the tip of the other wing to which the excitation is applied, using the Polytec Laser Doppler vibrometer PSV-500 Xtra 1D. The control subsystem is managed by the Raspberry Pi with the add-on boards MCC 128 and MCC 152 manufactured by Measurement Computing, dedicated respectively for acquisition and analog signal generation. A voltage divider is used to adjust the voltage measurement at PZT2 to the acquisition card limits of plus or minus 10V. The piezoelectric actuators in charge of the inductance variation are controlled by the signal generated in the MCC-152 card, which is amplified with a gain of 20 in the Cedrat XX power amplifier. The resonant circuit consisting only of the tunable inductor is connected to PZT2 and mounted right next to the aircraft prototype. The machine learning control algorithm for closed-loop operation in the experimental tests performed are implemented on the Raspberry Pi.

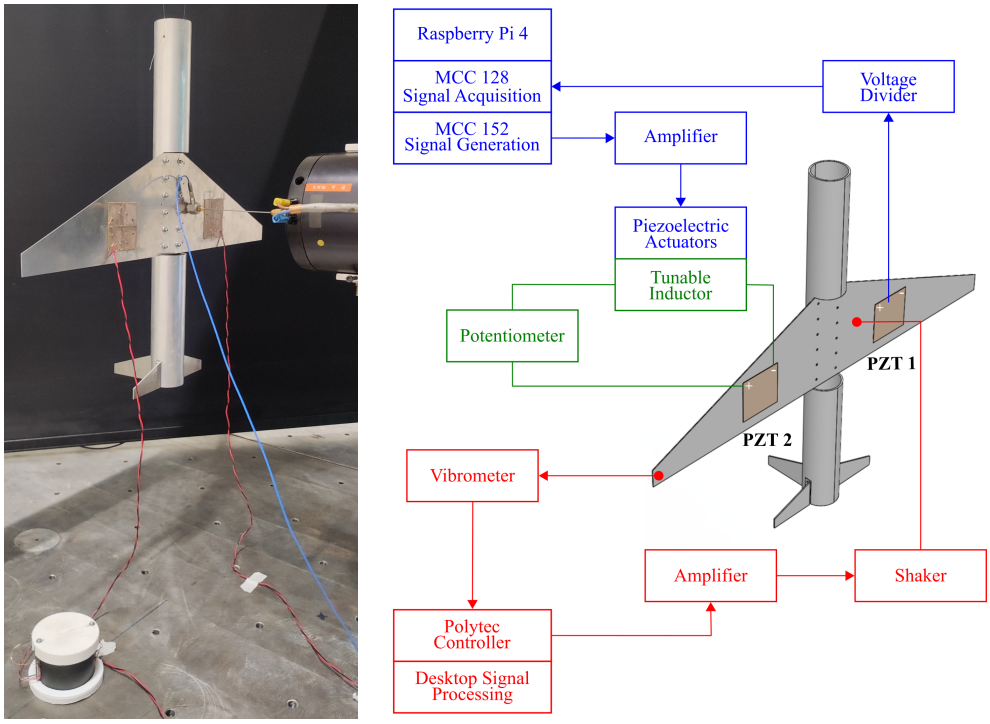

(a) (b)

Figure 6: Photograph of the experimental setup (a) and its schematic representation (b).

3.2. Design and manufacturing of tunable passive inductor

The position and dimensions of the piezoelectric patches shown in Figure 6 were chosen based on a parametric study of the finite element model of the aircraft prototype coupled

with the piezoelectric patches. This model of the prototype aircraft was recently explored in the study presented by Bachy et al. [43] with a different type of absorber, where more details about its formulation, material properties and dimensions are presented. The parametric study using this model was carried out by varying the position of the piezoelectric patches along the wings of the prototype. The position providing the maximum electromechanical coupling factor with respect to the third bending mode of the aircraft was chosen. The choice of this symmetric mode was based on a compromise between its frequency and the inductance required to tune the PVA. Note that a mode with a lower resonance frequency would be possible, but would require a higher inductance (see Equation 4) and would consequently increase the number of turns required for the same type of ferrite core, thus increasing the dimensions of the inductor. The width and length dimensions of the patches were chosen to maximize the piezoelectric capacitance, aiming to reduce the inductance required that, according to Equation 6, is inversely proportional to the piezoelectric capacitance.

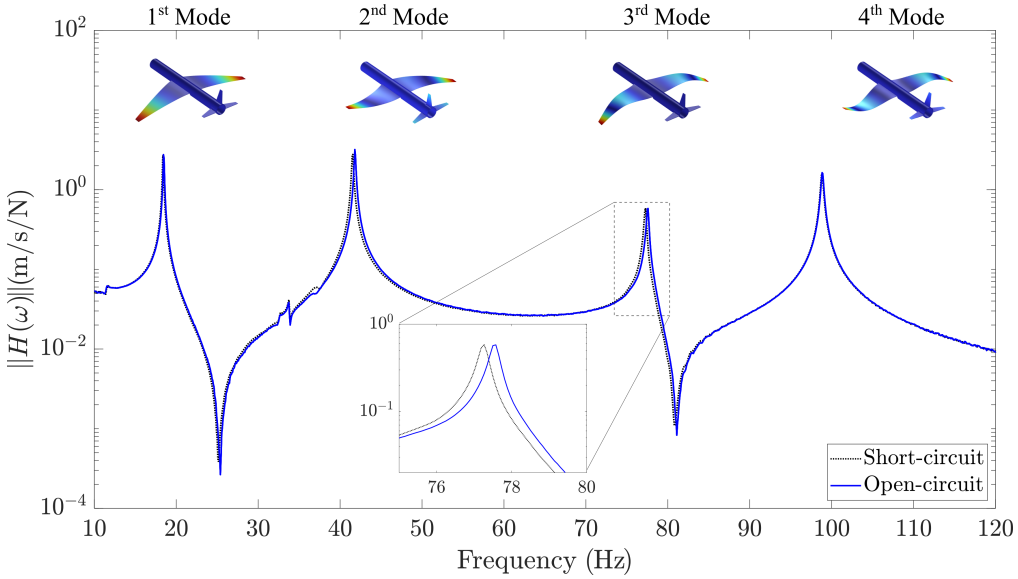

Figure 7: Mobility frequency response function and corresponding mode shapes for short-circuit and open-circuit patch configurations.

The initial design of the resonant circuit was performed considering constant inductance, given by Equation 6. The electromechanical coupling was estimated using Equation 3 and the natural frequencies obtained from the experimental FRFs shown in Figure 7 for the piezoelectric transducers in open-circuit and short-circuit conditions. The value of the piezoelectric capacitance at constant strain was measured experimentally using an impedance analyzer. From the estimated experimental parameters and using Equation 6, an inductance of 28.64 H and a resistance of 1533.18 Ω were obtained for the equal-peak design solution. All the numerical values are summarized in Table 1.

The inductance and resistance estimates for the solution based on the equal-peaks method was used as a starting point for the tunable inductor design. Among the various commercially available ferrite cores, the T26 ferrite was chosen because it offers a suitable

Table 1: Numerical values for the experimental estimated parameters.

ω_{oc}(Hz)	ω_{sc}(Hz)	k_c	C^{ε} (nF)	L_{ep} (H)	R_{ep} (Ω)	A_l (μH/tr^2)
77.56	77.25	0.0897	147	28.64	1533.18	10

compromise between inductance factor and maximum saturation current. Based on the initial values of inductance an resistance and the inductance factor supplied by the manufacturer of the T26 ferrite cores it is possible to calculate the number of windings required to make the coil, which was 1692 turns. However, since the tunable inductance is controlled by the air gap between the cores, which decreases the inductance as the air gap increases, the coil is made with a higher number of turns to allow the inductance to vary within a margin of plus or minus 10% of the calculated initial value. Thus, the coil was manufactured using an automatic winding machine with 1900 turns of 0.35 mm diameter copper wire. The inductor was assembled using the coil and the T26 ferrite cores along with piezoelectric stack actuators. The overall dimensions of the ferrite core are 70 mm in diameter and 42 mm in height. The inductance measured using a LCR meter for the assembled inductor without air gap between the cores was 35.5 H with a quality factor of 181.3, which is equivalent to a DC resistance of 95 Ω. A photograph of the tunable inductor including the fixed base and movable support additively fabricated using PLA and the piezoelectric actuators is shown in Figure 8(a).

The characterization of the relationship between the inductance and the applied voltage in the piezoelectric actuators was performed using the experimental setup schematized in Figure 8(b). A voltage generator was used to apply a constant signal varying from 0 to 5 V with a step of 0.5 V, while an LCR meter was used to measure the inductance at each level. This test was repeated three times and the results obtained are shown in Figure 8(c). Note in this curve that with increasing applied voltage, raising the space between the ferrite core proportionally, initially induces a linear variation in inductance. However, as the gap increases, the magnetic flux lines start to bulge out around the gap, causing a reduction in effective air gap reluctance and consequently an increase in inductance, a phenomenon known as the fringing effect, which explains the change in trend of the curve. For more details on fringing effect the interested reader can refer to [33, 35].

3.3. Self-adaptive control based on Gaussian Process Regression

The application of the proposed self-adaptive strategy requires an initial supervised learning step performed off-line. The aircraft prototype is submitted to an automated data collection process for training the GPR model. Using the test and control subsystem simultaneously, a constant amplitude harmonic excitation signal is applied to the shaker and the excitation frequency is varied from 70 to 85 Hz with a step of 0.5 Hz. For each frequency the voltage applied to the piezoelectric stack actuators is varied from 0 to 5 V with a step of 0.25 V, for a total of 651 test configurations. For each configuration the structure is excited for 2 seconds followed by 1s of rest, and the synchronized acquisition of the time signals of velocity measured by the vibrometer and voltage at the PZT1 is performed. This process,

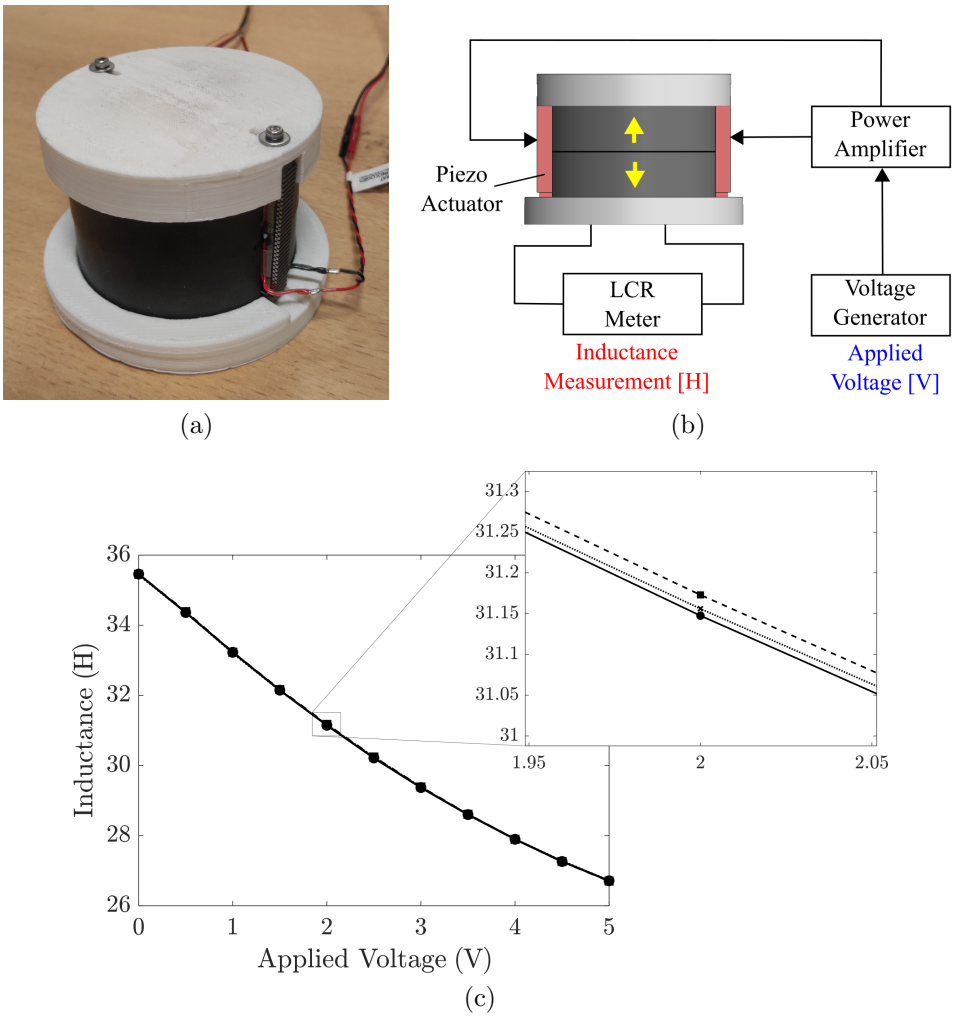

Figure 8: Experimental characterization of the semi-passive tunable inductor. Photograph of the (a) fabricated device, (b) schematic of the experimental setup used for the characterization, and (c) results of the experimental characterization of the variable inductance as a function of the voltage applied to the stack for the three tests performed: test 1 (- -), test 2 (—) and test 3 (····).

which is fully automated, takes approximately 32 minutes.

Samples of the time signals for the wing velocity measured by the vibrometer and voltage at PZT1 for an excitation frequency of 70 Hz and applied voltage on the piezoelectric actuators of 0 V are presented in Figure 9. The time-averaged RMS values of the signals for all experimentally tested conditions as a function of excitation frequency and applied voltage on the stack are represented through the surface plots presented in Figure 10. It can be observed by analyzing the surface presented in Figure 10(a) that the RMS value of the velocity has a smooth behavior in relation to the excitation frequency, with the existence of minimum operating points - highlighted by the blue dots - as a function of the voltage applied to the piezoelectric stack actuators, which controls the resonance frequency of the electric circuit. It is important to note that the minimum points for the velocity surface

coincide exactly with the minimum points for the voltage values in PZT 1. This is because the two surfaces have a remarkably similar shape. This fact can be quantitatively verified by calculating the distance between the two normalized surfaces, which have a maximum distance of 0.0028. Therefore, it allows the use of the voltage signal measured at PZT 1 to evaluate the cost function, which is considerably more practical for the implementation in practice than the velocity measured by the vibrometer, since the transducer is already installed in the structure and can be readily measured. The voltage measured on PZT sensor, which is proportional to its strain, is therefore in this case proportional to the velocity of the structure at the measured point. Hence, hereafter the measured velocity by the vibrometer will only be used for validation of the implemented control system.

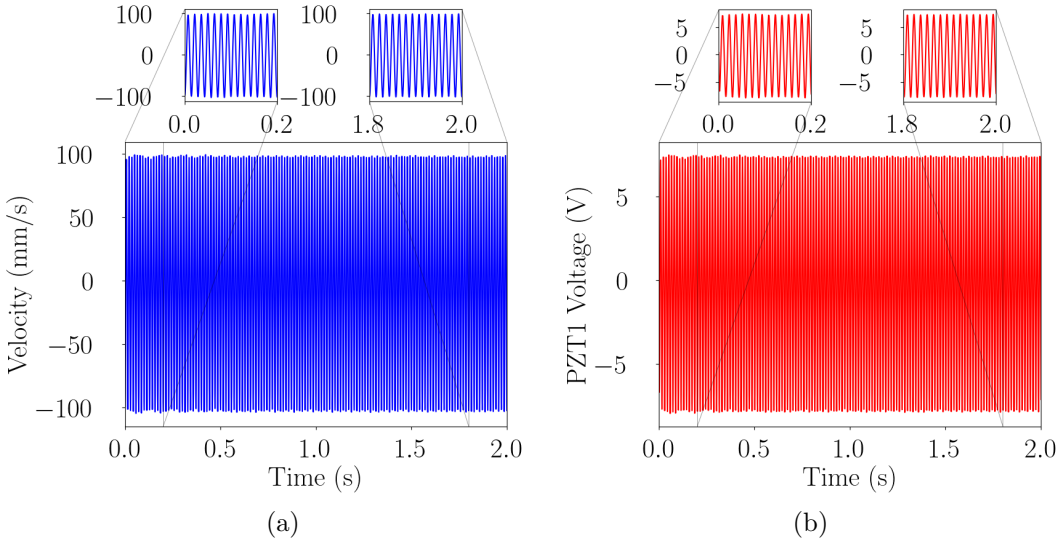

Figure 9: Time signals of (a) velocity at measured point by the vibrometer and (b) voltage in PZT 1 for 75 Hz excitation frequency and 0V applied to piezoelectric stack actuators.

A total of five tests were performed to collect experimental data with the 651 mentioned configurations. The data sets from four of these tests were used to train the GPR model, considering the excitation frequency and the applied voltage on the piezoelectric actuators as input variables and the RMS voltage value at PZT 1 as output. The experimental data used for training and the predicted mean of the trained model is presented in Figure 11. The model validation was performed using Root-Mean Squared Error (RMSE) criterion based on leave-one-out cross-validation method, for which the last data set from the five was used. The maximum RMSE between the RMS voltage of PZT 1 experimentally observed and predicted by the model obtained was of 0.038. This low RMSE value is a strong indicator of adequate prediction the trained GPR model.

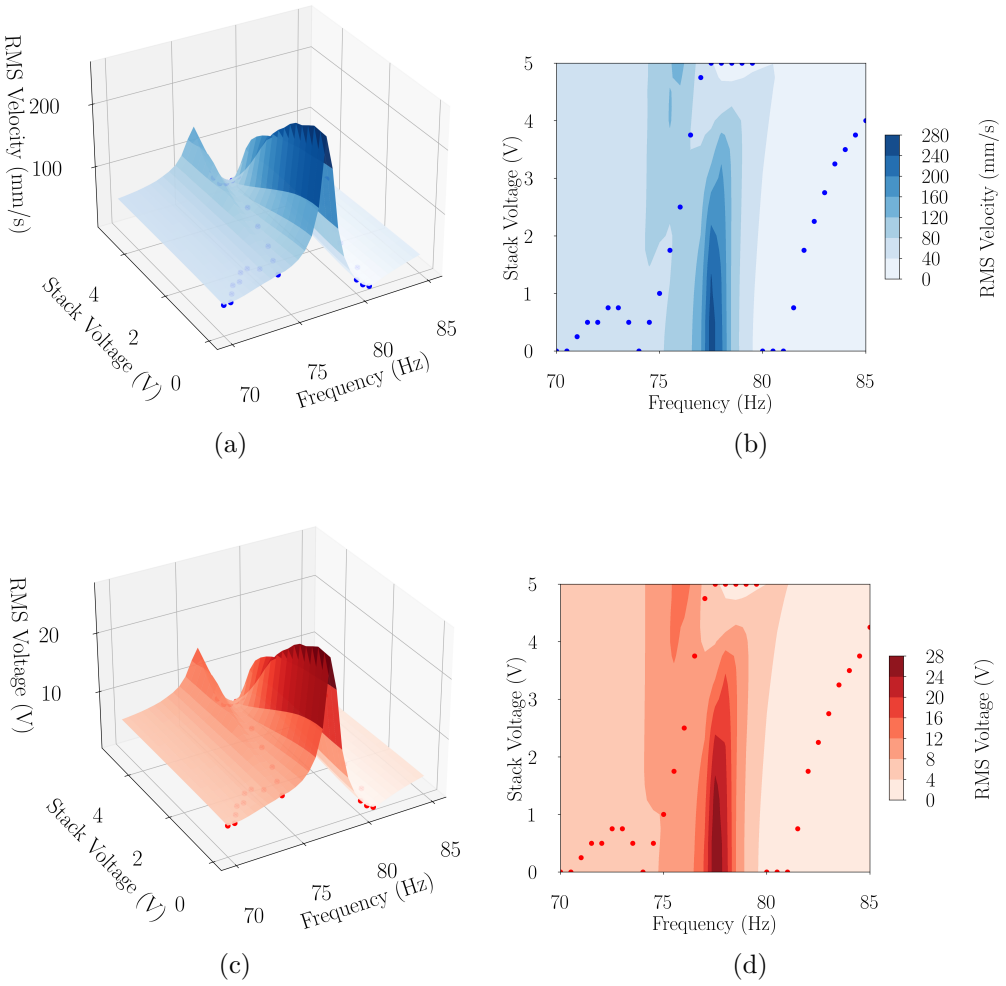

Figure 10: Experimental surfaces obtained for the RMS value of velocity (a)(b) and voltage at PZT 1 (c)(d) as a function of excitation frequency and applied voltage on the piezoelectric actuators for the first test performed.

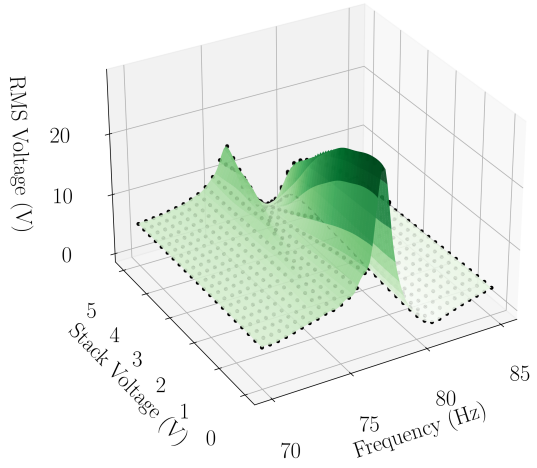

Figure 11: Predicted mean ( )by the GPR model trained with the experimental data (●) used for training from four of the five tests.

3.3.1. Closed-loop control based on the trained GPR model

Once the GPR model has been trained in the off-line learning loop, the self-adaptive control strategy can be tested in closed-loop. The test subsystem is used to excite the structure with a swept-sine signal with frequency varying linearly from 70 Hz to 85 Hz and a duration of 120 seconds. The machine learning control algorithm based on the trained GPR model is implemented on the Raspberry Pi, responsible for the control subsystem that runs independently. The voltage acquisition at PZT 1 is performed at a sampling frequency of 2500 Hz and with a duration of 0.5 s. For each voltage time signal acquired the frequency is estimated using the fast Fourier transform based on the parabolic interpolation approach. The signal frequency is then used as input to the GPR model, which is used to estimate the voltage that must be applied to the piezoelectric actuators to minimize the stress on PZT 1 and consequently the vibration in the structure. This whole process takes place in a closed-loop online on the Raspberry Pi board.

The experimental results of the self-adaptive control strategy is compared to the solution provided by the equal-peak design, in which the inductance is kept constant regardless of the operating conditions. This solution is obtained experimentally by adjusting the tunable inductance to the condition where the experimental FRF of the system has two equal-peaks around the mode of interest. It is important to note that the resistance of the shunt circuit was kept unchanged at 95 Ohms. The results obtained for these two strategies are presented in Figure 12. An attenuation gain of 3.07 dB (equivalent to an amplitude reduction of approximately 30%) is obtained by comparing the maximum amplitudes can be observed for the self-adaptive strategy for frequencies around the third mode, which can be explained by the antiresonance locus at the excitation frequency. In particular, at the resonant frequency of the mode of interest, the two solutions perform similarly, which is to be expected, since in this case the excitation frequency coincides with the frequency of the mode for which equal-peak method solution is based and the resistance of the shunt has not modified. It should be emphasized here that the purpose of this comparison is only to highlight the strategic difference between the two methodologies, since better vibration attenuation is already expected for harmonically excited structures from the self-adaptive methodology, which is based on the antiresonance localization strategy, compared to the equal-peaks methodology. The peak in the velocity response at $80s$ is due to the drastic decrease in the voltage applied to the piezoelectric actuators, causing a sharp decrease in inductance. This causes a transient response of the system, which soon reaches the steady-state response, but that should be further investigated.

The voltage signal applied to the tunable inductor has a relationship with the electrical resonance frequency of the shunt whose trend can be inferred from its inductance. With the increase of the applied voltage, it is expected a decrease in inductance (see Figure 8) and consequently an increase in the electric resonance frequency of the shunt (see Equation 4). Thus, the analysis of the time signal of the voltage applied to the actuators indicates that there was an overall increase in resonance of the electrical circuit from 0 to approximately 60 s, following approximately the same trend of the excitation frequency. However, one can question the behavior of the sharp reduction of the applied voltage around 80 s which indicates a reduction of the electric resonance frequency as the excitation frequency increases.

Although this behavior cannot be explained regarding the antiresonance locus strategy presented in the previous section for the lumped mass model, it is important to note that this experimental application involves a complex structure with multiple modes, some of which are close to each other (see mode 3 and 4 in Figure 7). Moreover, the nonlinear effects of the semi-passive tunable inductor as well as uncertainties, are difficult to take into account in the traditional model-based control approach. This justifies and strengthens the advantages of the model-free approach based on the machine learning control method presented here.

The machine learning control strategy proposed in this work is applicable for the operation of the structure under operating conditions within the conditions used in training of the GPR model, which limits its application in more challenging scenarios susceptible to unforeseen variations in environmental and operating conditions. However, recent works involving the use of GPR models has already shown the possibility of updating a trained model with data obtained during operation in a way that allows the adaptation of the controller in case of structural changes [44]. Alternatively, the application of gradient-based optimization methods for the online controlling of the input variable of the closed-loop system as applied in the past may be envisaged [10, 11]. This approach offers the advantages of not requiring a training phase as is the case in the machine learning approach, and of being adaptable in operation to the different sources of uncertainty affecting the system. However, they require a longer convergence time to a control solution for the system, which hinders their application in cases of time-varying harmonic signals such as those studied in this work.

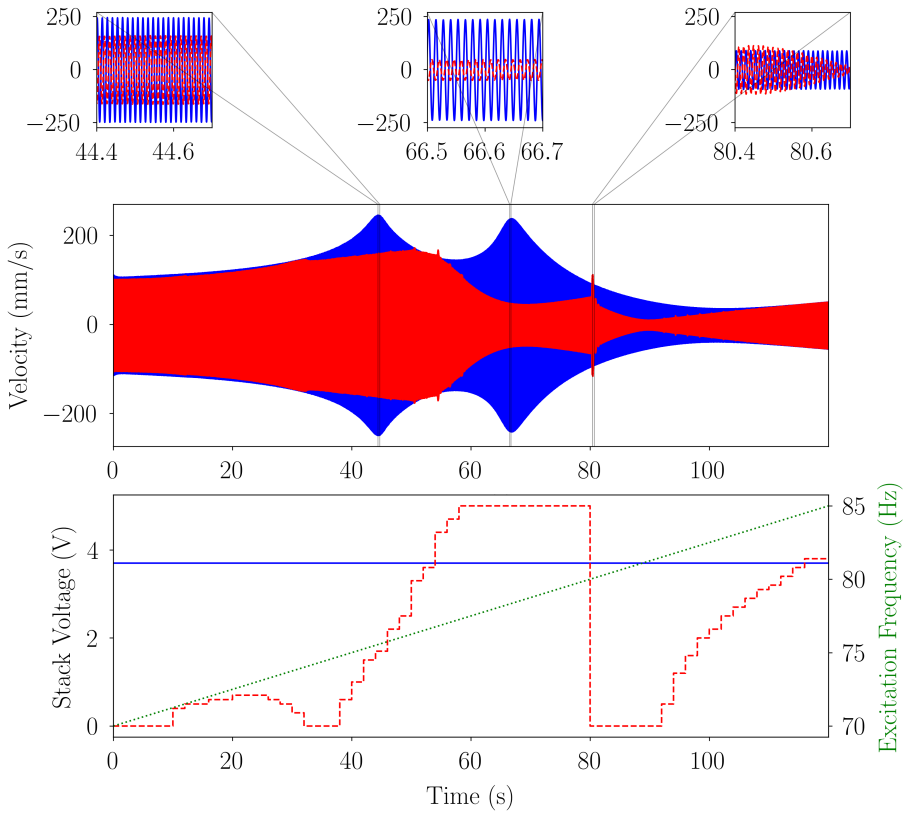

Figure 12: Closed-loop experimental application of the self-adaptive strategy based on the trained GPR model (- -) compared to the solution provided by the equal-peak method (—), in which inductance remains constant.The structure is excited with a swept-sine signal with frequency varying linearly (····) from 70 Hz to 85 Hz.

4. Conclusions

This paper proposed a self-adaptive PVA with semi-passive resonant shunt for used in the vibration attenuation of harmonically excited structures. This technique has many advantages. A resonant shunt composed only of passive components circumvents the main limitation of the widely used synthetic impedances, in particular the problem of instability. In addition, the inductance of the novel high-Q tunable inductor can be controlled by the application of a simple constant voltage signal, unlike the devices with similar capabilities based on SSD and PWM techniques that require signals at high-switching frequencies. Moreover, the proposed self-adaptive strategy based on machine learning control does not require a physical model of the closed-loop system since it employs a supervised learning approach via a GPR model to learn how to control the semi-passive tunable inductor to achieve the maximum vibration attenuation as function of the excitation frequency. The application of this strategy was demonstrated experimentally on a simplified airplane mockup. The results show a significant improvement of approximately 3.07 dB (equivalent to an amplitude reduction of approximately 30%) in vibration attenuation for a swept sine excitation compared to a traditional resonant shunt with fixed inductance. Future applications to the

attenuation of vibrations in rotating machinery are envisaged as well as an extension to the case of broadband frequency excitations.

Acknowledgments

This work has been supported by the EUR EIPHI Project (contract ANR-17-EURE-0002), Bourgogne Franche-Comté Region.

Declaration of interest

The authors declare that they have no known competing financial interests or personal relationships that could have appeared to influence the work reported in this paper.

References

[1] J. Gripp, D. Rade, Vibration and noise control using shunted piezoelectric transducers: A review, Mech. Syst. Signal Process. 112 (2018) 359–383. https://doi.org/10.1016/j.ymssp.2018.04.041.

[2] R. L. Forward, Electronic damping of vibrations in optical structures, Appl. Opt. 18 (5) (1979) 690–697. https://doi.org/10.1364/AO.18.000690.

[3] N. W. Hagood, A. v. Flotow, Damping of structural vibrations with piezoelectric materials and passive electrical networks, J. Sound Vib. 146 (2) (1991) 243–268. https://doi.org/10.1016/0022-460X(91)90762-9.

[4] P. Soltani, G. Kerschen, G. Tondreau, A. Deraemaeker, Piezoelectric vibration damping using resonant shunt circuits: An exact solution, Smart Mater. Struct. 23 (12), publisher: IOP Publishing. https://doi.org/10.1088/0964-1726/23/12/125014.

[5] S.-M. Kim, S. Wang, M. J. Brennan, Dynamic analysis and optimal design of a passive and an active piezo-electrical dynamic vibration absorber, J. Sound Vib. 330 (4) (2011) 603–614. https://doi.org/https://doi.org/10.1016/j.jsv.2010.09.004.

[6] O. Thomas, J. Ducarne, J.-F. Deü, Performance of piezoelectric shunts for vibration reduction, Smart Mater. Struct. 21 (1) (2012) 015008. https://doi.org/10.1088/0964-1726/21/1/015008.

[7] U. Andreaus, M. Porfiri, Effect of electrical uncertainties on resonant piezoelectric shunting, J. Intell. Mater. Syst. Struct. 18 (5) (2007) 477–485. https://doi.org/10.1177/1045389X06067116.

[8] R. Darleux, B. Lossouarn, J. F. Deü, Passive self-tuning inductor for piezoelectric shunt damping considering temperature variations, J. Sound Vib. 432 (2018) 105–118. https://doi.org/10.1016/j.jsv.2018.06.017.

[9] J. J. Hollkamp, J. Thomas F. Starchville, A self-tuning piezoelectric vibration absorber, J. Intell. Mater. Syst. Struct. 5 (4) (1994) 559–566. https://doi.org/10.1177/1045389X9400500412.

[10] A. J. Fleming, S. O. R. Moheimani, Adaptive piezoelectric shunt damping, Smart Mater. Struct. 12 (1) (2003) 36. https://doi.org/10.1088/0964-1726/12/1/305.

[11] D. Niederberger, A. Fleming, S. O. R. Moheimani, M. Morari, Adaptive multi-mode resonant piezoelectric shunt damping, Smart Mater. Struct. 13 (5) (2004) 1025. https://doi.org/10.1088/0964-1726/13/5/007.

[12] J. A. B. Gripp, L. C. S. Góes, O. Heuss, F. Scinocca, An adaptive piezoelectric vibration absorber enhanced by a negative capacitance applied to a shell structure, Smart Mater. Struct. 24 (12) (2015) 125017. https://doi.org/10.1088/0964-1726/24/12/125017.

[13] P. Gardonio, G. Konda Rodrigues, L. Dal Bo, E. Turco, Extremum seeking online tuning of a piezoelectric vibration absorber based on the maximisation of the shunt electric power absorption, Mech. Syst. Signal Process. 176 (2022) 109171. https://doi.org/10.1016/j.ymssp.2022.109171.

[14] G. Konda Rodrigues, P. Gardonio, L. Dal Bo, E. Turco, Piezoelectric patch vibration control unit connected to a self-tuning RL-shunt set to maximise electric power absorption, J. Sound Vib. 536 (2022) 117154. https://doi.org/10.1016/j.jsv.2022.117154.

[15] C. Richard, D. Guyomar, D. Audigier, G. Ching, Semi-passive damping using continuous switching of a piezoelectric device, in: T. T. Hyde (Ed.), Smart Structures and Materials 1999: Passive Damping and Isolation, Vol. 3672, International Society for Optics and Photonics, SPIE, 1999, pp. 104 – 111. https://doi.org/10.1117/12.349773.

[16] M. Lallart, S. Harari, L. Petit, D. Guyomar, T. Richard, C. Richard, L. Gaudiller, Blind switch damping (BSD): A self-adaptive semi-active damping technique, J. Sound Vib. 328 (1-2) (2009) 29–41. https://doi.org/10.1016/j.jsv.2009.07.030.

[17] A. Faiz, L. Petit, D. Guyomar, J. Ducourneau, A new adaptive resonance frequency of piezoelectric components used for vibration damping, J. Acoust. Soc. Am. 127 (4) (2010) EL134–EL139. https://doi.org/10.1121/1.3327238.

[18] L. Dal Bo, P. Gardonio, D. Casagrande, S. Saggini, Smart panel with sweeping and switching piezoelectric patch vibration absorbers: Experimental results, Mech. Syst. Signal Process. 120 (2019) 308–325. https://doi.org/10.1016/j.ymssp.2018.10.024.

[19] M. Auleley, O. Thomas, C. Giraud-Audine, H. Mahé, Enhancement of a dynamic vibration absorber by means of an electromagnetic shunt, J. Intell. Mater. Syst. Struct. 32 (3) (2021) 331–354. https://doi.org/10.1177/1045389X20957097.

[20] M. Auleley, C. Giraud-Audine, H. Mahé, O. Thomas, Tunable electromagnetic resonant shunt using pulse-width modulation, J. Sound Vib. 500 (2021) 116018. https://doi.org/10.1016/j.jsv.2021.116018.

[21] A. Antoniou, Realisation of gyrators using operational amplifiers, and their use in rc-active-network synthesis, Proc. Inst. Electr. Eng. 116 (1969) 1838–1850(12).

[22] R. Riordan, Simulated inductors using differential amplifiers, Electron. Lett. 3 (1967) 291–291(0).

[23] G. Raze, A. Jadoul, S. Guichaux, V. Broun, G. Kerschen, A digital nonlinear piezoelectric tuned vibration absorber, Smart Mater. Struct. 29 (1) (2019) 015007. https://doi.org/10.1088/1361-665X/ab5176.

[24] K. Dekemele, P. V. Torre, M. Loccufier, High-voltage synthetic inductor for vibration damping in resonant piezoelectric shunt, J. Vib. Control 27 (17-18) (2021) 2047–2057. https://doi.org/10.1177/1077546320952612.

[25] G. Raze, Piezoelectric digital vibration absorbers for multimodal vibration mitigation of complex mechanical structures, Ph.D. thesis, University of Liege (2021).

[26] M. P. Deisenroth, D. Fox, C. E. Rasmussen, Gaussian processes for data-efficient learning in robotics and control, IEEE Trans. Pattern Anal. Mach. Intell. 37 (2) (2015) 408–423. https://doi.org/10.1109/TPAMI.2013.218.

[27] L. Hewing, J. Kabzan, M. N. Zeilinger, Cautious model predictive control using gaussian process regression, IEEE Trans. Control Syst. Technol. 28 (6) (2020) 2736–2743. https://doi.org/10.1109/TCST.2019.2949757.

[28] X. Wang, D. Wang, F. Li, Y. Zhang, Z. Xu, T. Wang, G. Fu, C. Lu, Self-learning vibration absorber with negative electromagnetic stiffness for variable vibration, Int. J. Mech. Sci. 248 (2023) 108225. https://doi.org/10.1016/j.ijmecsci.2023.108225.

[29] H. Song, X. Shan, L. Zhang, G. Wang, J. Fan, Research on identification and active vibration control of cantilever structure based on NARX neural network, Mech. Syst. Signal Process. 171 (2022) 108872. https://doi.org/10.1016/j.ymssp.2022.108872.

[30] M. Maiworm, Gaussian process in control : model predictive control with guarantees and control of scanning quantum dot microscopy, Ph.D. thesis, Otto-von-Guericke-Universität Magdeburg, Fakultät für Elektrotechnik und Informationstechnik (2021).

[31] M. Maiworm, C. Wagner, R. Temirov, F. S. Tautz, R. Findeisen, Two-degree-of-freedom control combining machine learning and extremum seeking for fast scanning quantum dot microscopy, in: 2018 Annual American Control Conference (ACC), 2018, pp. 4360–4366. https://doi.org/10.23919/

ACC.2018.8431022.
[32] B. Lossouarn, M. Aucejo, J. F. Deu, B. Multon, Design of inductors with high inductance values for resonant piezoelectric damping, Sens. Actuators A: Phys. 259 (2017) 68–76, publisher: Elsevier B.V. https://doi.org/10.1016/j.sna.2017.03.030.
[33] V. Valchev, A. Van den Bossche, Inductors and Transformers for Power Electronics, 1st Edition, CRC Press, Boca Raton, 2018.
[34] R. Darleux, Development of analogous piezoelectric networks for the vibration damping of complex structures, Ph.D. thesis, HESAM Université (2020).
[35] M. Frivaldsky, M. Pipiska, M. Zurek-Mortka, D. Andriukaitis, PFC Inductor Design Considering Suppression of the Negative Effects of Fringing Flux, Appl. Sci. 12 (13) (2022) 6815. https://doi.org/10.3390/app12136815.
[36] T. Duriez, S. L. Brunton, B. R. Noack, Machine Learning Control – Taming Nonlinear Dynamics and Turbulence, Fluid Mechanics and Its Applications, Springer International Publishing, Cham, 2017.
[37] P. Fleming, R. Purshouse, Evolutionary algorithms in control systems engineering: a survey, Control Eng. Pract. 10 (11) (2002) 1223–1241. https://doi.org/10.1016/S0967-0661(02)00081-3.
[38] S. L. Brunton, J. N. Kutz, Data-Driven Science and Engineering: Machine Learning, Dynamical Systems, and Control, 1st Edition, Cambridge University Press, 2019.
[39] R. Li, B. R. Noack, L. Cordier, J. Borée, F. Harambat, Drag reduction of a car model by linear genetic programming control, Exp. Fluids 58 (8) (2017) 103. https://doi.org/10.1007/s00348-017-2382-2.
[40] C. E. Rasmussen, C. K. I. Williams, Gaussian Processes for Machine Learning, The MIT Press, 2006.
[41] K. Worden, P. Green, A machine learning approach to nonlinear modal analysis, Mech. Syst. Signal Process. 84 (2017) 34–53, recent advances in nonlinear system identification. https://doi.org/10.1016/j.ymssp.2016.04.029.
[42] M. Gasior, J. L. Gonzalez, Improving FFT Frequency Measurement Resolution by Parabolic and Gaussian Spectrum Interpolation, AIP Conf. Proc. 732 (1) (2004) 276–285. https://doi.org/10.1063/1.1831158.
[43] E. Bachy, K. Jaboviste, E. Sadoulet-Reboul, N. Peyret, G. Chevallier, C. Arnould, E. Collard, Investigations on the performance and the robustness of a metabsorber designed for structural vibration mitigation, Mech. Syst. Signal Process. 170 (2022) 108830. https://doi.org/10.1016/j.ymssp.2022.108830.
[44] A. Cully, J. Clune, D. Tarapore, J. B. Mouret, Robots that can adapt like animals, Nat. 521 (7553) (2015) 503–507. https://doi.org/10.1038/nature14422.